Single ions in Paul traps

H. C. Nägerl[1,2], Ch. Roos[1], H. Rohde[1], D. Leibfried[1], J. Eschner[1], F. Schmidt-Kaler[1], and R. Blatt[1]

[1] Institut für Experimentalphysik, Universität Innsbruck, Technikerstraße 25, A-6020 Innsbruck, Austria
[2] California Institute of Technology, Dept. of Physics (12-33), 1200 E. California Blvd., Pasadena, CA 91125, USA

Abstract. The use of cold trapped ions for quantum information processing requires the preparation of linear strings of ions at low temperatures and the coherent manipulation by laser light of the quantum state of individual ions in the string. In our experiment, $^{40}Ca^{+}$ ions are trapped in a linear Paul trap, forming crystallized linear strings when laser cooled. These strings are observed by fluorescence detection on the $S_{1/2}$ - $P_{1/2}$ dipole transition at 397nm using a photomultiplier and a CCD camera. The narrow $S_{1/2}$ - $D_{5/2}$ quadrupole transition at 729nm is used to investigate and manipulate the vibrational motion of the ion in the trap. The spectral resolution obtained up to now on this transition is $2 \cdot 10^{-12}$, proving long coherence time of the two-level system. Addressing of individual ions in the string is achieved, using a tightly focused laser beam at 729nm, and detected by the observation of quantum jumps from the $S_{1/2}$ to the $D_{5/2}$ level. These experimental techniques make ions in a superposition of their $S_{1/2}$ and $D_{5/2}$ states suitable as qubits for quantum information processing. The realization of a two-ion quantum gate furthermore requires ground-state cooling of the string. The status of current experiments is reviewed and techniques to achieve ground-state cooling of ion strings are discussed. The application of those techiques including coherent control of the full quantum state of the ion string will lead in future to systematic investigations of decoherence.

1 Introduction

One or a few ions stored in a radio-frequency Paul trap offer an ideal environment to study the dynamics of simple quantum systems. With the aid of laser pulses, the investigator can taylor the interaction of this system almost at will. Quantum information processing, as well as the study of foundations of quantum mechanics, ultrahigh precision spectroscopy, and the investigation of future frequency standards, and last but not least the investigation of decoherence, are possible applications of the perfect control of internal and external quantum mechanical degrees of freedom of a string of trapped ions [1–5]. A particulary interesting situation arises when a suitable laser light field couples the motion of the ion(s) in the trapping potential with their electronic levels. This situation is described by an interaction Hamiltonian acting on two internal electronic levels, $|s\rangle$ and $|d\rangle$, with energy difference

ω_{sd}, which are 'dressed' by the harmonic oscillator states $|n\rangle$ of the external motion at frequency ω_{trap} (see Fig. 1).

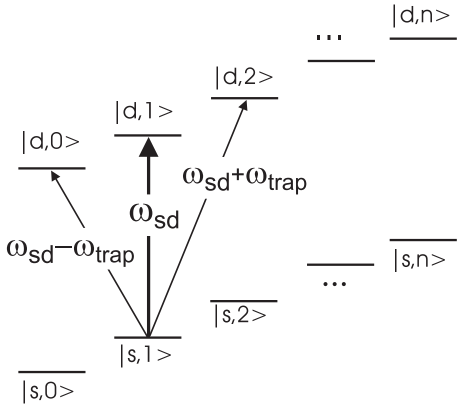

Fig. 1. Electronic states of a two-level atom $|s\rangle$ and $|d\rangle$, 'dressed' by the number states of its quantized motion.

The interaction Hamiltonian takes the form

$$H_{\text{int}} = -\hbar\Omega\left(\sigma^{+}e^{i\eta(a^{\dagger}+a)} + \sigma^{-}e^{-i\eta(a^{\dagger}+a)}\right), \tag{1}$$

where $\eta = k\sqrt{\hbar/2m\omega_{trap}}$ is the Lamb-Dicke parameter, $(a^{\dagger}+a)$ the position operator in terms of creation and annihilation operators for the harmonic oscillator, and Ω is the coupling strength proportional to the amplitude of the laser light field. This interaction Hamiltonian is inherently richer than the classical Jaynes Cummings Hamiltonian [6–9], but reduces to the latter in the so-called Lamb-Dicke limit

$$\eta \cdot \sqrt{\langle(a^{\dagger}+a)^2\rangle} = \eta \cdot \sqrt{2n+1} << 1 \tag{2}$$

and when the detuning of the light field with respect to ω_{sd} is $\delta = -\omega_{trap}$. We assume that the radiative width of both levels $|s\rangle$ and $|d\rangle$ is much smaller than ω_{trap}, such that the motional sidebands of the atomic resonance, $|s,n\rangle$ to $|d,n\pm1\rangle$, are well resolved. In general, any detuning $\delta = (n'-n)\cdot\omega_{trap}$ (n, n' integer numbers) will resonantly drive transitions between the states $|s,n\rangle$ and $|d,n'\rangle$, and thus lead to a different interaction Hamiltonian.

2 Ion trapping

The experimental techniques to realize a well controlled situation [10–16] described by the Hamiltonian above have historically evolved from efforts to build frequency standards with trapped and cooled ions [17–19]. Dynamical trapping of charged particles in radiofrequency (rf) traps has been first proposed and experimentally verified by W. Paul in 1958 [20]. An rf electric field, generated by an appropriate electrode structure, creates a pseudo-potential confining a charged particle [21]. For the trapping of single ions the electrodes typically have dimensions of a few millimeters down to about 100 μm. The rf fields are in the 1-300 MHz range, with amplitudes of hundreds of Volts. The motion of a particle confined in such a field consists of a fast component synchronous with the applied driving field (micromotion), which disappears at the node of the rf field, and a slow (secular) motion in the dynamically created pseudo-potential. For a quadrupole rf field geometry, the pseudo-potential is harmonic and the quantized secular motion of the trapped ion is very accurately described by a quantum harmonic oscillator.

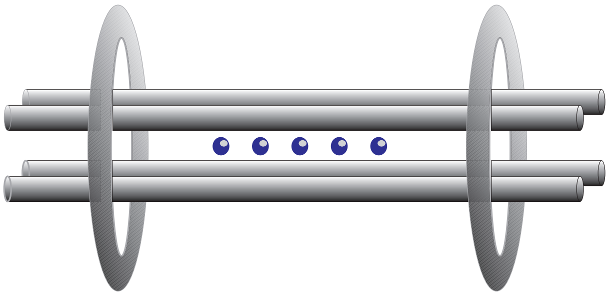

Fig. 2. Schematic setup of the linear trap. Confinement is maintained by the rf quadupole field in radial direction and by the dc potential of positively charged ring electrodes.

In a *linear* Paul trap, the quadrupole rf field exists only in the xy-plane, such as in a quadrupole mass spectrometer, and an additional electrical dc potential provides confinement along the z-axis (see Fig. 2). A major advantage compared to a three-dimensional Paul trap is that the micromotion completely vanishes for all ions on the z-axis. Furthermore the oscillation frequency in that direction can be chosen freely and independently from the radial secular frequencies. In contrast, in three-dimensional Paul traps Coulomb repulsion between ions pushes them into the rf field where micromotion heating occurs. Linear Paul traps presumably avoid completely this heating source even for long linear strings of ions. However, even if the use of linear traps for a larger number of ions seems favorable, an elongated version of the three-dimensional Paul trap has been used to produce strings of two and three ions [22].

Our trap [23] consists of 4 parallel steel rods with 2mm spacing, diagonally connected to generate the quadrupole rf field for radial confinement. The rf field at $\Omega/2\pi = 18$MHz yields a radial trapping pseudo-potential with secular frequencies of ω_r =1.4MHz. Two DC ring electrodes of 4mm diameter and 10mm spacing serve as the axial endcaps for longitudinal confinement. DC voltages on the ring electrodes result in a harmonic trapping potential at an axial frequency of ω_z =100 - 500kHz. The relatively large dimensions of our trap help to reduce unwanted interactions between the ion string and surface charges on the electrodes and thus reduce heating [24]. Ions are produced from an atomic beam by electron impact ionization inside the trap, where they are subsequently confined and laser cooled [25,26].

3 Laser cooling

We have chosen $^{40}Ca^+$ ions for the experiments since their excitation wavelengths are relatively easy to generate with solid state and diode lasers. See Fig. 3 for the relevant energy levels. Laser light at 397nm is generated with a frequency doubled Ti:Sapphire laser at 793nm while the light sources at 866nm, 854nm and 850nm are grating stabilized diode lasers. For Doppler cooling of the Ca^+ ions we use the dipole-allowed $S_{1/2}$-$P_{1/2}$ transition at 397nm, and we reach a temperature near the Doppler cooling limit of 0.5mK. Fluorescence light of the ions at 397nm is collected through two optical viewports using f/1.3 collimation lenses at a working distance of 65mm. One lens images the spatially integrated fluorescence onto a photomultiplier, and the second lens images the ion string onto an intensified CCD camera with 20-fold magnification. Here we observe linear ion strings of up to 15 ions, with distances between the ions of 19μm (2 ions) to 7μm (15 ions). See Fig. 4 for an image of 1, 2, 3, 9, and 10 ions. The optical resolution for the detection of fluorescence light at 397nm has been measured to be 4μm [23].

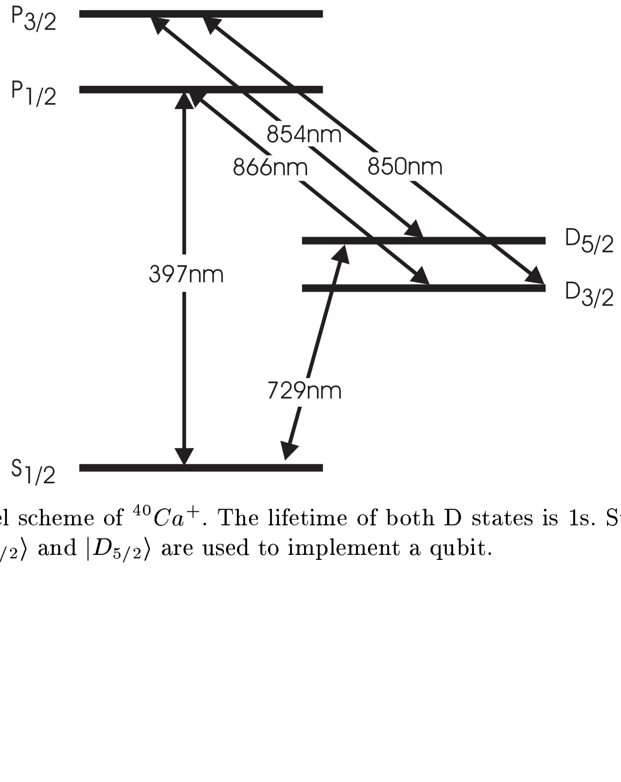

Fig. 3. Level scheme of $^{40}Ca^+$. The lifetime of both D states is 1s. Superposition states of $|S_{1/2}\rangle$ and $|D_{5/2}\rangle$ are used to implement a qubit.

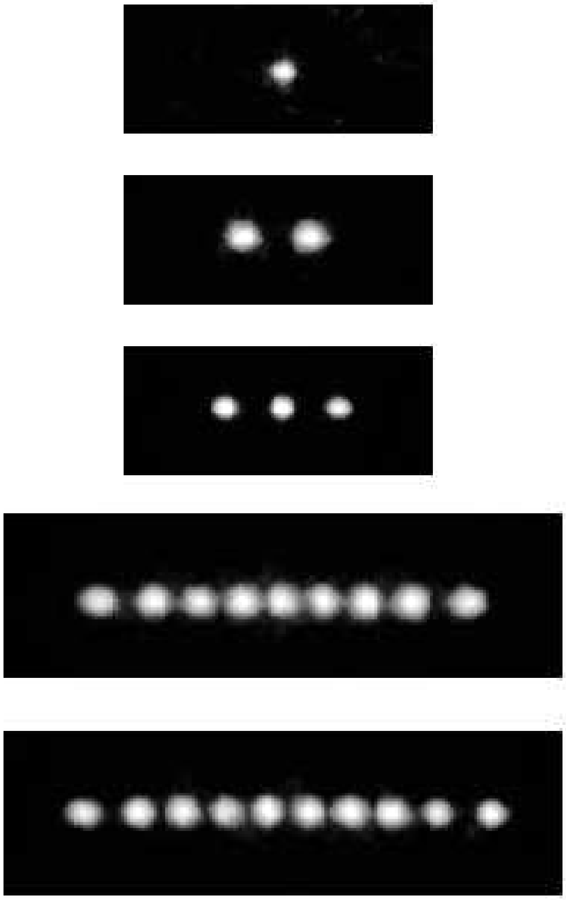

Fig. 4. Examples of linear strings of ions at ω_z=125kHz, leading to a distance between two ions of 19μm. The exposure time of the CCD camera was 1s.

Further cooling [22,28,27] beyond the Doppler limit of 0.5mK is possible in the $^{40}Ca^+$ ion by sideband cooling on the quadrupole $S_{1/2}$-$D_{5/2}$ transition at 729nm. A highly frequency stabilized Ti:Sapphire laser generates the light to excite this transition. Additionally, we shine light at 854nm onto the ions to quench the metastable $D_{5/2}$ state and thus increase the cooling rate. Please note that sideband cooling is much simpler if the initial state after Doppler cooling is well within the Lamb-Dicke regime, see Fig. 5. This condition is easily fulfilled if the trap frequency in z-direction is above 500kHz such that $\eta_{effective} = \eta \cdot \sqrt{2\langle n\rangle_{therm.}+1} \leq 1$ and the average vibrational quantum number at the Doppler limit is $\langle n\rangle_{therm.} \leq 20$.

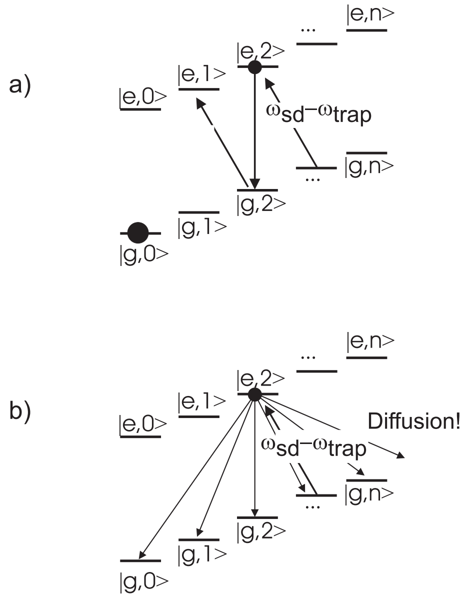

Fig. 5. a) Scheme of sideband cooling inside the Lamb-Dicke regime. The cooling laser is red detuned from the bare atomic resonance by ω_{trap}. b) red sideband excitation outside the Lamb-Dicke limit leads to strong diffusion and heating.

4 Normal modes of oscillation

In a linear ion trap, ions can be confined and optically cooled such that they form ordered structures [29,30]. If the radial confinement is strong enough such that $\omega_r/\omega_z > 0.73N^{0.86}$, N ions arrange in a linear string along the trap axis at distances determined by the equilibrium of their Coulomb repulsion and the axial dc potential. If this potential is sufficiently harmonic, the positions can be described by a single parameter, the axial frequency ω_z. Small displacements of the ions from their equilibrium positions are described in terms of normal modes. As an example, consider two $^{40}Ca^+$ ions confined in a linear ion trap: The first normal mode corresponds to an oscillation of both ions moving together back and forth as if they were rigidly joined. This oscillation is referred to as the *center-of-mass* (COM) *mode* of the string. The second normal mode corresponds to an oscillation where the two ions move in opposite directions. More generally, this so-called *breathing-mode* describes a string of N ions moving with an amplitude proportional to their mean distance from the trap center. Explicit calculation of the normal modes and the respective eigenfrequencies of an ion string yields the following results [32,33]: i) for a one-dimensional string consisting of N ions there are N normal modes and normal frequencies, ii) the frequency of the center of mass mode is equal to the frequency of a single ion, iii) higher order frequencies are nearly independent of the ion number N and are given by (1, $\sqrt{3}$, $\sqrt{29/5}$, 3.05(2),...)·

ω_z, where the numbers in brackets indicate the maximum frequency deviation as N is increased from 1 to 10 ions, iv) the relative amplitudes of the normal modes have to be evaluated numerically, at least for strings with more than 3 ions, see equation (28) in Ref. [32].

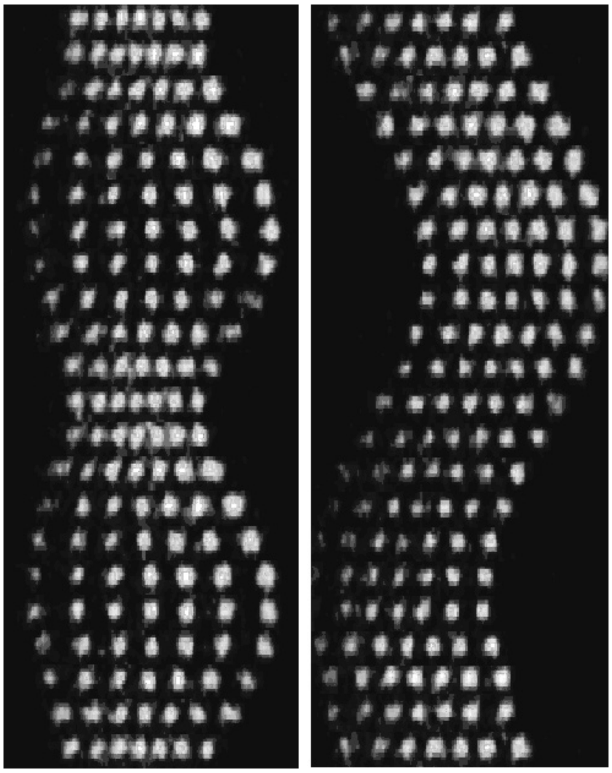

Fig. 6. Stroboscopic image of the rf-excited center-of-mass motion at 158.5kHz (right) and breathing mode motion at 276.0kHz (left). For animated pictures see also [16]

After loading the trap with a string of ions, we excited normal modes by applying additional ac-voltages to one of the ring electrodes [31]. The normal mode oscillation has been observed stroboscopically with the gated CCD camera that accumulates images at the same phase of the exciting electric field. The measured excitation frequency for the breathing mode agrees within 1% with the expected frequency of $\sqrt{3}$ times the center-of-mass frequency. Fig. 6 shows the excitation of the center of mass mode (158.5 kHz) for a string of seven ions and the excitation of the breathing mode (276.0 kHz). In order to excite the breathing mode it was necessary to apply voltages about 300 times higher than the ones needed for excitation of the center of mass mode. Excitations of higher order modes other than the breathing mode were not observed with the available ac-voltages. This is due to the fact that the exciting field is nearly uniform along the ion string so that higher modes, which need field parallel to the ion chain are excited much less efficiently. The COM vibration is excited with a uniform field and is therefore very susceptible to field fluctuations. In contrast, the excitation of higher order modes by field fluctuations is less likely since the spatial field variation is very small on the length scale given by the ion distance. Therefore, this unwanted heating process occurs less strongly for the higher order modes.

5 Electron shelving

The basic idea of the 'electron shelving' method as proposed by Dehmelt [34] is very simple: It requires a three-level system consisting of a ground state $|s\rangle$, a metastable excited state $|d\rangle$, and a short lived excited state $|p\rangle$. A laser pulse couples the ground state to the excited state $|d\rangle$, leaving the system in a superposition $\alpha|s\rangle+\beta|d\rangle$. If now the $|s\rangle \rightarrow |p\rangle$ transition is driven, the short lived state $|p\rangle$ will be excited and scatter photons if, and only if, the system collapses into $|s\rangle$. The state reduction already happens with the first scattered photon even if it is not observed. The measurement yields the result $|s\rangle$ with probability $|\alpha|^2$, corresponding to the observation of photons, or the result $|d\rangle$ with probability $|\beta|^2$, corresponding to the absence of photons. Even if the efficiency for detecting the photon from one decay of $|p\rangle$ is low (typically 10^{-3}) one can keep re-exciting the system and scatter millions of photons, eventually detecting a few of them in case the state is reduced to $|s\rangle$. If the state is 'shelved' in the metastable state $|d\rangle$, no fluorescence will occur. In every single experiment the answer will be either $|s\rangle$ - photons detected - or $|d\rangle$ - no photons detected - , thus distinguishing these states with 100 % detection efficiency and destroying all coherences between them. Averaged over many experiments, the number of tries where fluorescence photons are observed will be proportional to $|\alpha|^2$.

As an example of the efficiency of this method, Fig. 7 shows the fluorescence signal from a single Ca^+ ion during continuous excitation on the $S_{1/2} \rightarrow P_{1/2}$ transition at 397 nm and the $\mathrm{S}_{1/2} \rightarrow D_{5/2}$ transition at 729 nm. While the ion is in the $\mathrm{S}_{1/2}$ or $P_{1/2}$ state it radiates about 2000 photons in 100 ms into the photomultiplier. At certain times, the ion is excited into the $\mathrm{D}_{5/2}$ state by the beam at 729 nm and the rate drops to about 150 events in 100 ms, given by the number of dark counts of the imperfect photomultiplier, and some 397 nm light directly scattered from the exciting beam into the detector. Obviously, the two states can be discriminated with excellent precision already within one ms. The average dark time is about 1 second, the radiative lifetime of the $\mathrm{D}_{5/2}$ state. In the language of quantum information processing, this two-level system of $\mathrm{S}_{1/2}$ state and $\mathrm{D}_{5/2}$ state represents an ideal qubit, several of them form a quantum register. For such a possible realization of a quantum register, the observation of fluorescence with the intensified CCD camera yields the internal state detection with 100 % probability: The sites of the ions in the string appear bright or dark depending on the logic state of each qubit.

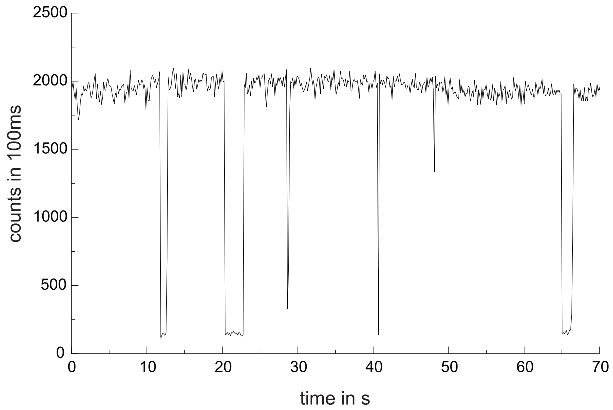

Fig. 7. Quantum jumps of a single $^{40}Ca^{+}$ ion. When the ion makes a transition to the metastable $D_{5/2}$ state, the fluorescence drops. After an average time equal to the lifetime of the excited state ($\tau \simeq 1$ s), a spontaneous transition returns the ion to the ground state and the fluorescence reappears.

6 Spectroscopy of the $S_{1/2} - D_{5/2}$ transition

For quantum information processing, the dressed quantum states of the qubits are coherently manipulated using laser pulses similar to the $\pi/2$-pulses used in optical Ramsey spectroscopy. To investigate this technique with a single ion, we first used laser pulses of fixed length at 729nm that couple the $S_{1/2}$ and $D_{5/2}$ states. A magnetic field is used to split the transitions to different m_J levels in frequency. After preparing the $S_{1/2}, m_J = +1/2$ sub-state by optical pumping, we excite the ion to the $D_{5/2}$ state manifold of Zeeman sublevels. We are mainly interested in the $S_{1/2} \rightarrow D_{5/2}, m_J = +1/2 \rightarrow +5/2$ transition which has the largest Clebsch-Gordon coefficient. In the third step of this 'quantized spectroscopy', see Fig. 8, we detect whether a transition to the shelving level $D_{5/2}$ has been induced.

The above sequence is repeated typically 100 times to measure the excitation probability P_D for any set of parameters. In this way we study the dependance of P_D on experimental parameters such as the detuning of the light at 729nm with respect to the ionic transition or the length of the excitation pulse. The duration of a single sequence is typically 5ms or less, and we can synchronize the sequence with the ac power line at 50Hz, which reduces ac-magnetic field fluctuations, although at the cost of slower data aquisition. As a consequence of the harmonic ladder of 'dressed' ion states

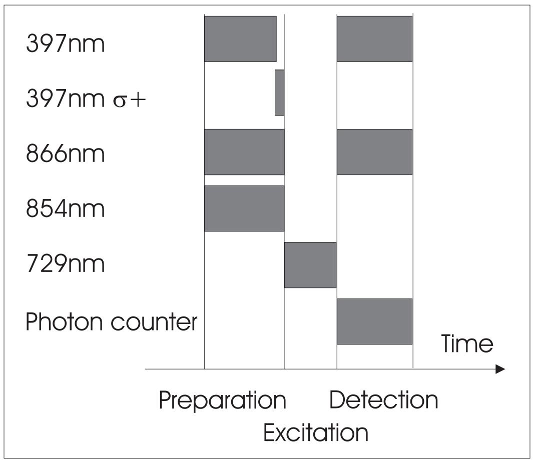

Fig. 8. Experimental sequence for the quantized spectroscopy, see text for details.

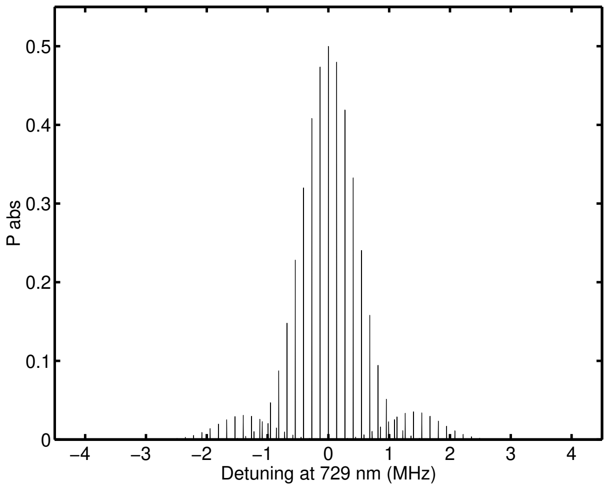

Fig. 9. Calculated sideband spectrum for excitation of the $S_{1/2}$ to $D_{5/2}$ transition, for one ion below saturation and at the Doppler cooling limit. Oscillation frequencies are ω_z=136kHz, ω_r=1.4MHz. The radial sidebands are magnified by a factor of 10.

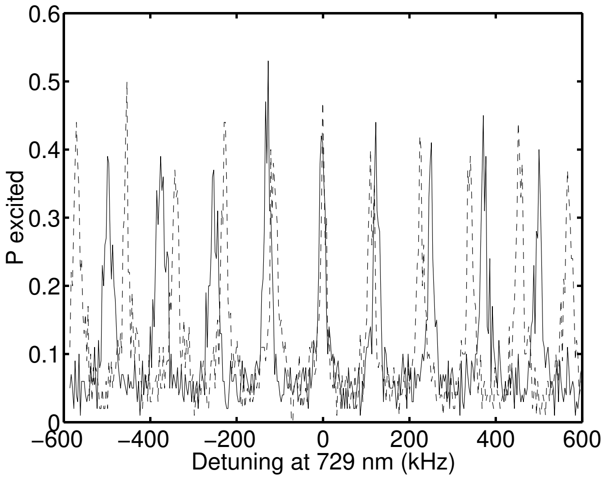

Fig. 10. Shift with trap frequency of the low-order sidebands adjacent to the carrier, as observed with one ion. The dashed line shows the spectrum as measured with a trap stiffness corresponding to ω_z=113.8kHz. For the solid line, the ring voltages were increased by about 10V, resulting in an increase of ω_z to 124.1kHz. No ac-power line synchronization was used.

(Fig. 1), the spectrum of excitation $P_D(\nu)$ vs δ_{729}, Fig. 9, shows a central peak with equidistant sidebands at multiples of the trap frequencies. The width of the envelope corresponds to the ion temperature that was assumed for this simulation to be at the Doppler limit of 0.5mK and η=0.25. The measured sideband spectra in Fig. 10 show equidistant sidebands at the trap frequency on the z-axis. Increasing the voltages on the ring -shaped endcap electrodes increases the trap frequency. The only resonance that does not shift corresponds to excitation on the carrier frequency (without change in phonon number: n $\rightarrow$ n). The observed linewidth for the transition on the carrier has been measured to be 1kHz ($\delta\nu/\nu = 2 \cdot 10^{-12}$) in the ac-power-line synchronized aquisition mode. The inverse of this measured linewidth, 1ms, gives the upper limit for any coherent operation, and we are currently working to further improve this limit. The main limitations are the fluctuations of the magnetic field at the ions position and the phase fluctuations of the Ti:Sappire laser at 729nm.

7 Driving coherent dynamics

A major requirement for quantum information processing is the ability to apply laser pulses of certain duration to implement qubit rotations of $\pi/2$, π and 2π [4]. We have experimentally varied the pulse length of excitation on the carrier and measured the $D_{5/2}$ state probabilty $P_D(t)$ (see Fig. 11).

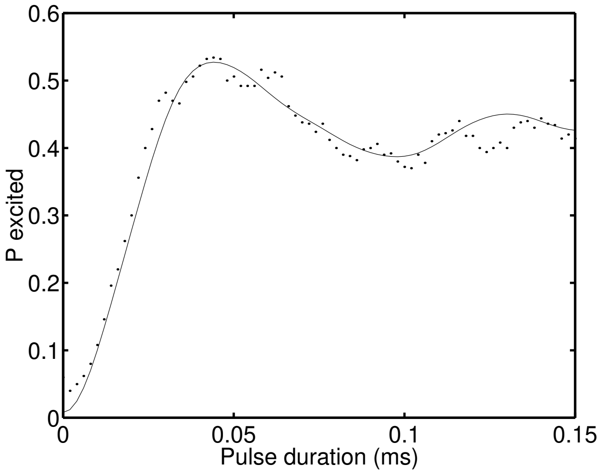

Fig. 11. Rabi oscillations between $|S_{1/2}, n\rangle$ and $|D_{5/2}, n\rangle$ for a single ion in the linear trap. The solid curve is a plot of equation (3) with Lamb-Dicke parameter η=0.25, Rabi frequency $\Omega = 2\pi\cdot$ 50kHz, and thermal occupation number $\langle n_{therm.}\rangle$=500.

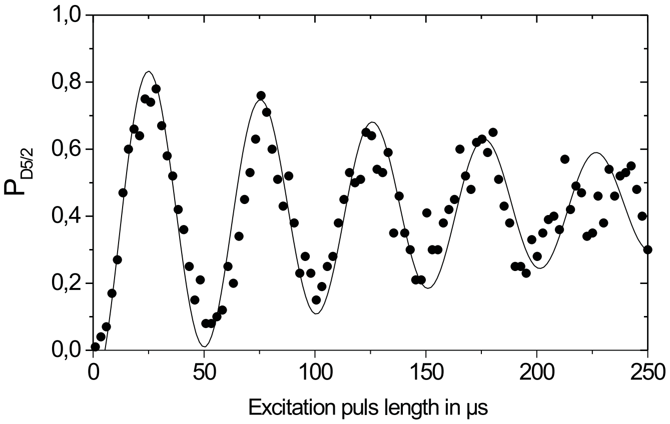

Fig. 12. Rabi oscillations as in Fig. 11, measured in a three-dimensional Paul trap with higher trap frequency ω = 0.9MHz with a single Doppler cooled ion. The solid curve is calculated with η=0.09, $\Omega = 2\pi\cdot$ 11.4kHz, and $\langle n_{therm.}\rangle$=11.6. The Doppler cooling limit for this trap is $\langle n\rangle$=11

The theoretical curve which fits the data takes the different Rabi frequencies Ω_{nn} for the transitions $|s,n\rangle$ to $|d,n\rangle$ into account.

$$P_D(t) = \sum_{n=0}^{\infty} p_n \cdot \sin^2(\Omega_{nn} \cdot t), \tag{3}$$

$$\Omega_{nn} = \Omega \cdot e^{-\eta^2/2} \cdot \mathcal{L}_n^0(\eta), \tag{4}$$

where p_n denotes the phonon probability distribution and $\mathcal{L}_n^0$ a Laguerre polynomial. The oscillating dependence of Ω_{nn} on n and the large mean thermal vibration number $\langle n \rangle$, as is typical for the relatively weak z-confinement of the linear Paul trap, are responsible for the fast dephasing we observe. Here, after Doppler cooling, the ion is *not* found in the Lamb-Dicke regime. We emphasize that the dephasing is *not* due to laser frequency fluctuations which limit coherent dynamics only on a timescale of 1ms. This is also proven by a similar measurement of Rabi oscillations that we performed in a three-dimensional single ion Paul trap with much tighter binding (see Fig. 12). Four Rabi oscillation periods are clearly visible and the dephasing is again mainly due to the summation of different frequencies Ω_{nn}.

In a series of exciting experiments, the ion storage group around D. Wineland has used coherent dynamics for the generation and investigation of nonclassical phonon states [35], the implementation of a controlled-NOT gate [36], measurements of the Wigner function [37], and experiments on Schrödinger cat states temporal decoherence [38].

8 Individual addressing of ions in a string

Taking advantage of the high optical resolution of the lens for the collection of fluorescence in our experiment, we use the same optical path also for individual addressing (see Fig. 13). The ingoing laser beam at 729nm is separated from the outgoing uv fluorescence with a dichroic mirror. An optical fiber between laser and trap setup provides stable alignment, and a telescope is used to adjust the λ=729nm beam parameters for optimum focusing. Between fiber exit and telescope, an acousto-optical modulator (AOM 1) is used to shift the direction of the addressing beam and thus to allow focusing onto the different ions. The ion string is illuminated by the addressing laser under an angle of $\alpha = 67.5$ degrees to the trap axis in order to allow qubit excitation together with excitation of vibrational modes at frequency ω_z. In this geometry, we calculate a Lamb-Dicke parameter $\eta = k \cdot \sqrt{\hbar \cos^2(\alpha)/2m\omega_z}$ =0.17 for the center-of-mass motion.

We have experimentally demonstrated two ways of addressing single ions in the string with a string of 3 ions [39]: First, we used the tightly focused 729nm laser beam at a fixed position and shifted the ion string by slight variation (less than 1%) of the endcap ring electrode voltages while the variation of the ion string position was monitored on the CCD camera. Secondly,

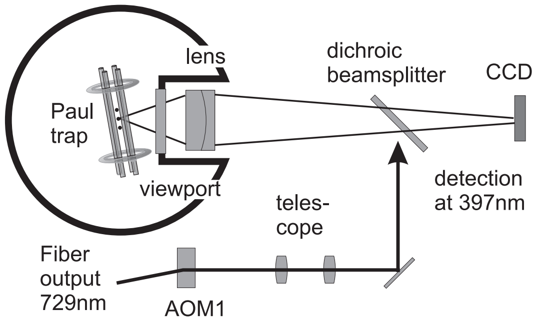

Fig. 13. Scheme of the experimental setup to address single ions in a string. Laser light at 729nm from an optical fiber is superimposed with the (counterpropagating) fluorescence at 397nm on a dichroic beamsplitter. Thus, the laser is focused by the objective lens onto the ion string. A two-lens telescope transforms the fiber output for optimum focussing. To address different ions in the string, either the acousto-optical modulator (AOM1) is used to shift the direction of the laser beam, or the ions are shifted with additional dc potentials on the ring electrodes.

we fixed the ion string position and moved the laser beam over the string with the AOM1. The optical excitation sequence consists of three parts: A 0.5ms excitation period with light at 729nm is followed by a detection period with the laser at 397nm and 866nm on (2ms), during which we register the quantum jump probability P_D to the metastable $D_{5/2}$ level. The sequence is closed by a cooling and repumping period with the lasers at 397nm, 866nm and 854nm on (2ms). During the excitation period, we use a weak beam at 397nm to spectrally broaden the narrow $S_{1/2}$ - $D_{5/2}$ transition. This excitation sequence is repeated 100 times, thus yielding a value for the P_D. The average of 15 such measurements is plotted versus the center position of the ion string in Fig. 15.

From a fitted Gaussian function $A_0 + \sum A_i \exp[-2((x - x_i^0)/w_i)^2]$ with height A_i, position x_i^0, and width w_i corresponding to the three peaks in the signal and background A_0, we obtain a spatial resolution of addressing of w=5.6(0.2)μm. This width of the Gaussian is mostly due to the optical properties of the addressing channel, since the Ca^+ ion wave packet has a calculated width of $\sqrt{\delta x^2}$=1.6μm at 5mK. For exact calibration of the CCD pixel size we used a resonant excitation of the center-of-mass mode of the ion string [31] (see section IV). From the measured frequency of 125(0.2)kHz we obtain an equilibrium distance between the ions of 19.12(0.02)μm [32]. Thus, we can exactly calibrate the pixel size of the recorded CCD images to 1.12μm per pixel. In Fig. 15 (b) - (d) we show CCD images of the addressed string, with different ions transferred to the non-fluorescing $D_{5/2}$ state. Assuming a Gaussian intensity distribution, the intensity of the addressing beam at the position of a neighbouring ion 9μm away would be as small as 1%. After having shown sufficiently good spatial resolution for individual addressing, we

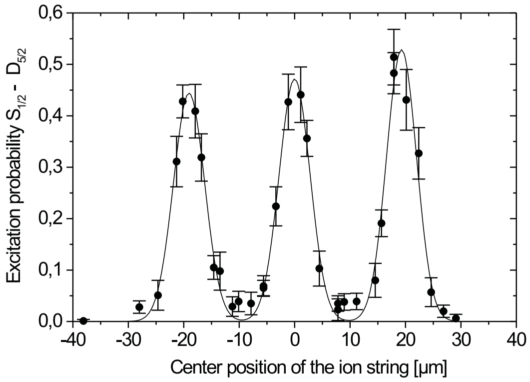

Fig. 14. Quantum jump rate from the $S_{1/2}$ to the $D_{5/2}$ state induced by a tightly focused laser beam at 729nm. The ion string position is varied while the laser waist remains fixed. Individual ions are resolved by the addressing beam with a Gaussian width of w $=5.6(0.2)\mu$m. See Fig. 15 for CCD images of the string that were taken simultaneously. The error bars indicate the one sigma deviations from 15 measurements.

implemented a scheme that would be directly applicable to future quantum information processing. Shifting the ion string does not allow sufficiently fast switching for longer ion strings, since a fast, non-adiabatic shift of position would presumably cause heating [24]. For fast addressing, the laser beam position is shifted by an acousto-optical modulator (AOM 1) and thus focused on different ions. The associated change in frequency is compensated by a second double-pass acousto-optical modulator in front of the fiber. We measured an addressing resolution as good as in the first addressing scheme using static fields.

9 Decoherence of 'dressed' ion states

In section VII we have seen the dephasing of Rabi oscillations, which mimics decoherence. Technical noise such as the fluctuations of electromagnetic fields at the ions place, or laser phase noise also lead to reduced visibility in quantum interference experiments. In this chapter, however, we will concentrate on the two more fundamental sources of decoherence, these are the decay of the internal electronic state and the external vibrational state ('heating').

Decoherence of electronic hyperfine ground states of $^9Be^+$ has been tested e.g. in experiments by J. Bollinger [40] with stored ions in a Penning trap. Here, for the case of hyperfine ground states, the spontaneous decay is neglible and coherence of a qubit was maintained for more than 10s. In the case of optical transitions between ground state and a metastable excited states such

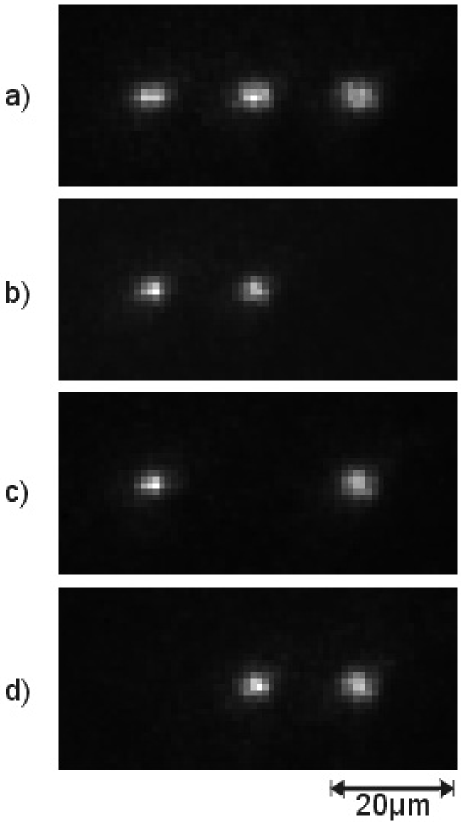

Fig. 15. (a): Fluorescence at 397nm of three ions imaged onto the CCD camera. The distance between ions is 19.12(0.02)μm (ω_z =125(0.2)kHz) and the spatial resolution is near 4μm. The exposure time is 1s. (b) - (d): Different ions in the string are addressed with focused laser light at 729nm and transferred into the non-fluorescing $D_{5/2}$ state.

as in $^{199}Hg^+$: $S_{1/2}$ - $D_{5/2}$ at 282nm, J. Bergquist reached a linewidth of ≈ 80Hz [41], corresponding to a decoherence time of several ms, which was still limited by phase fluctuations of the exciting laser source, and not by spontaneous decay of the excited state.

In traps, those electronic states are dressed by the vibrational quantum state, which in practice leads to stronger limitations. Heating rates of single ions in three-dimensional Paul traps have been measured for a relatively large trap with r ≈ 0.5mm at a trap frequency of $\omega_r \approx$ 3MHz with 6 phonons per s [28]. In later experiments with smaller three-dimensional Paul traps (r ≈ 0.17mm, $\omega \approx$ 10-20MHz), heating rates of even 1 phonon per ms have been observed [27]. A detailed theoretical and experimental study of different heating processes can be found in Ref. [24]. However, for linear strings, higher order modes show *heating orders of magnitude less* than for the fundamental center-of-mass mode. For two ions, $\langle dn/dt \rangle \approx 19$ phonons per ms for the center-of-mass mode has been measured while only $\langle dn/dt \rangle$ less than 0.18 phonons per ms have been found for the breathing mode [22]. Due to their coupling only to the *gradient* of an electric stray field (see Section IV) higher order modes show less heating and will be useful if long coherence times become necessary.

10 Conclusion

Currently, we modify our linear Paul trap for Ca^+ ions to find optimum conditions for individual addressing *and* sideband cooling. The obtained addressing resolution permits us to work with higher longitudinal trap frequencies of 500kHz - 1MHz at inter-ion distances of 8 - 6μm. With such trapping parameters we are in the Lamb-Dicke regime already after Doppler cooling. Switching between ions within a few μs is feasible and will allow roughly 10 operations on different ions within the coherence time of 1ms that we measured from high resolution spectroscopy on the $S_{1/2}$ - $D_{5/2}$ transition [42]. Stored ions in three-dimensional or linear Paul traps provide a versatile tool for quantum information processing. Systematic experimental studies of decoherence have only started recently [5,38,43]. We have given a description of experimental techniques for the storage, observation, cooling, individual addressing, and coherent manipulation of ions in linear strings. For future experiments, the advantages of ion trapping techniques such as - scalabilty from 1 to N ions in a string, the use of different vibration modes, long coherence times, and the 100% state detection probability - seem to be very promising for quantum information processing.

This work is supported by the Fonds zur Förderung der wissenschaftlichen Forschung (FWF) as project No. P11467 and within the Spezialforschungsbereich SFB 15, and in parts by the TMR networks "Quantum Information" (ERB-FMRX-CT96-0087), and "Quantum Structures" (ERB-FMRX-CT96-0077).

References

1. A. Ekert, in Atomic Physics **14**, 450, ed. D. J. Wineland, C. Wieman, S. J. Smith, AIP New York 1995.
   S. Haroche, et. al., in Atomic Physics **15**, 1.
   J. I. Cirac, S. Gardiner, T. Pellizari, J. Poyatos, P. Zoller, et. al., in Atomic Physics **15**, 16.
   D. J. Wineland et. al., in Atomic Physics **15**, 31.
   ed. H. B. van den Heuvell, J. T. M. Walraven, M. W. Reynolds , AIP New York 1996.

2. The Physics of Quantum Information, ed. D. Bouwmeester, A. Ekert, A. Zeilinger, Springer Berlin (1999), submitted.
3. A. Ekert and R. Josza, Rev. Mod. Phys. **68**, 3733, (1997).
4. J. I. Cirac, P. Zoller, Phys. Rev. Lett. **74**, 4091 (1995).
5. J. R. Anglin, J. P. Paz, and W. H. Zurek, Phys. Rev. A **55**, 4041 (1997).
6. C. A. Blockey, D. F. Walls, H. Risken, Europhys. Lett. **17**, 509 (1992).
7. J. I. Cirac, R. Blatt, A. S. Parkins, and P. Zoller, Phys. Rev. Lett. **70**, 762 (1993).
8. J. I. Cirac, R. Blatt, A. S. Parkins, and P. Zoller, Phys. Rev. A **49**, 1202 (1994).
9. J. I. Cirac, R. Blatt, and P. Zoller, Phys. Rev. A **49**, R3174 (1994).
10. http://www.bldrdoc.gov/timefreq/ion/index.htm
11. http://horology.jpl.nasa.gov/research.html
12. http://mste.laser.physik.uni-muenchen.de/lg/worktop.html
13. http://p23.lanl.gov/Quantum/quantum.html
14. http://dipmza.physik.uni-mainz.de/ www_werth/calcium/c alcium.html
15. http://www-phys.rrz.uni-hamburg.de/home/vms/group_a/in dex.html
16. http://heart-c704.uibk.ac.at/
17. Proc. 5th Symp. Freq. Standards and Metrology, ed. J. C. Bergquist, (World Scientific, 1996).
18. D.J. Berkeland, J.D. Miller, J.C. Bergquist, W.M. Itano, and D.J. Wineland, Phys. Rev. Lett.**80**, 2089 (1998).
19. R. Blatt, in Atomic Physics **14**, 219, ed. D. J. Wineland, C. Wieman, S. J. Smith, AIP New York 1995.
20. W. Paul, O. Osberghaus, and E. Fischer, Forschungsberichte des Wirtschafts- und Verkehrsministerium Nordrhein-Westfalen **415** (1958).
21. P. K. Ghosh, Ion traps, Clarendon, Oxford 1995.
22. B.E. King, C.J. Myatt, Q.A. Turchette, D. Leibfried, W.M. Itano, C. Monroe, and D.J. Wineland, Phys. Rev. Lett. **81**, 1525, (1998).
23. H. C. Nägerl, W. Bechter, J. Eschner, F. Schmidt-Kaler, and R. Blatt, Appl. Phys. B 66, 603 (1998).
24. D.J. Wineland, C. Monroe, W.M. Itano, D. Leibfried, B. King, and D.M. Meekhof, Journal of Research of the National Institute of Standards and Technology **103**, 259 (1998).
25. D. J. Wineland, W. M. Itano, J. C. Bergquist, and R. G. Hulet, Phys. Rev. A **36**, 2220, (1987).
26. D. J. Wineland, and H. Dehmelt, Bull. Am. Phys. Soc. **20**, 637 (1975).
27. C. Monroe, D. M. Meekhof, B. E. King, S. R. Jeffers, W. M. Itano, D. J. Wineland, P. Gould, Phys. Rev. Lett. **74**, 4011 (1995).
28. F. Diedrich, J. C. Bergquist, W. M. Itano, D. J. Wineland, Phys. Rev. Lett. **62**, 403 (1989).
29. I. Waki, S. Kassner, G. Birkl, H. Walther, Phys. Rev. Lett. **68**, 2007 (1992).
30. M. G. Raizen, J. M. Gilligan, J. C. Bergquist, W. M. Itano, D. J. Wineland, Phys. Rev. A **45**, 6493 (1992).
31. H. C. Nägerl, D. Leibfried, F. Schmidt-Kaler, J. Eschner, and R. Blatt, Optics Express **3**, 89, (1998).
32. D. F. V. James, Appl. Phys. B **66**, 181 (1998).
33. A. Steane, Appl. Phys. B **64**, 623 (1997),
34. H. Dehmelt, Bull. Am. Phys. Soc. **20** 60 (1975).
35. D.M. Meekhof, C. Monroe, B.E. King, W.M. Itano, and D.J. Wineland, Phys. Rev. Lett **76**, 1796 (1996).

36. C. Monroe, D. M. Meekhof, B. E. King, W. M. Itano, D. J. Wineland, Phys. Rev. Lett. **75**, 4714 (1995).
37. D. Leibfried, D.M. Meekhof, B.E. King, C. Monroe, W.M. Itano, and D.J. Wineland, Phys. Rev. Lett **77**, 4281 (1996).
38. C. Monroe, D.M. Meekhof, B.E. King, and D.J. Wineland, Science **272**, 1131 (1996).
39. H. C. Nägerl, D. Leibfried, G. Thalhammer, J. Eschner, F. Schmidt-Kaler, and R. Blatt, Phys. Rev. A (July 1999), in press.
40. J. J. Bollinger, J. D. Prestage, W.M. Itano, and D.J. Wineland, Phys. Rev. Lett **54**, 1000 (1985).
41. J. C. Bergquist, F. Dietrich, W.M. Itano, and D.J. Wineland, "Laser Spectroscopy IX", Springer and
J. C. Bergquist, F. Diedrich, W.M. Itano, and D.J. Wineland, in "Frontiers in Laser Spectroscopy" proc. International School of Physics "Enrico Fermi" Course CXX, ed. by T. W. Hänsch and M. Ingusio (North Holland, Amsterdam, 1994) pp. 359.
42. H. C. Nägerl, et. al. to be published
43. M. Brune, E. Hagley, J. Dreyer, X. Maître, A. Maali, C. Wunderlich, J.M. Raimond, and S. Haroche, Phys. Rev. Lett. **77**, 4887 (1996).